Influence of the Cobalt Active Site Neighbours in NiCo Nanocatalysts for Phosphine-Assisted Silane Activation

Anthony Ropp, Sophie Carenco

Influence of the Cobalt Active Site Neighbors in NiCo Nanocatalysts for Phosphine-Assisted Silane Activation

Anthony Ropp,[1] *Dr. Sophie Carenco,*[1,*]

[1] Sorbonne Université, CNRS, Laboratoire de Chimie de la Matière Condensée de Paris (LCMCP), 4 place Jussieu, 75005 Paris, France

E-mail: sophie.carenco@sorbonne-universite.fr; https://sophiecarenco.cnrs.fr/ ; ORCID : 0000-0002-6164-2053

Abstract

NiCo nanoparticles are active catalysts for a number of reactions, as an interesting alternative to noble metals. In particular, phosphine-covered NiCo nanoparticles with a 1:1 metal ratio were found to be active at room temperature for Si–H bond activation. However, it was unclear which of the two metals was the active site and if the neighboring atoms influenced the reaction efficiency. We designed nanoparticles with a nickel core and a limited amount of cobalt surface sites, just below or just above a monolayer amount, to investigate this question. We showed that the trend in catalytic activity is consistent with cobalt being the active site, and it shows a higher activity when its immediate neighbors are cobalt atoms. This was consistently observed with two phosphine ligands, PPh_3 and P*n*Bu_3, while the first allowed a higher conversion rate than the second.

Keywords: bimetallic nanoparticles, cobalt, hydrosilylation, nanocatalysis, nickel

Introduction

Bimetallic heterogeneous catalysts have attracted tremendous attention from the 1960s. Associating two metals proved to be a successful strategy to enhance both activity and selectivity of given chemical reactions.[1] More than only combining the properties of both metals, it often resulted in new properties through promotional effects.[2] The development of bimetallic nanoparticle syntheses yielding in morphologically well-defined nanoparticles led to a better understanding of the synergies between metals which stem from electronic and geometric effects.[2,3] Depending on the procedures and the miscibility of metals, either alloys, Janus-like, heterostructures or core-shell nanoparticles could be obtained.[4,5] As a result of the nanoparticle morphology, surface's geometry and composition can be tuned so that active sites are diluted or even isolated.[6–8]

Combinations of transition metals (Fe, Co, Ni, Cu) sometime present a catalytic activity competitive with these of scarce and expensive platinoid catalysts, which stimulated their investigations. In particular, variously shaped nickel-cobalt nanoparticles were applied as catalysts for many reactions such as methane dry reforming,[9–13] hydrogenations,[14–18] lignin depolymerization,[19] water splitting[20] and aldehyde hydrosilylation.[21] For example, while nickel alone is highly active for methane dry reforming, it rapidly deactivates because of coke formation. The alloying with cobalt results in reduced sensitivity to coking because of its ability to remove carbon deposits by oxidation.[12] Moreover, coke diffusion was accelerated on the NiCo alloy, reducing the poisoning of Ni active site. The alloying leads to electronic effects which decrease the bonding strength between Nickel and coke.[13]

Molecular additives also have a huge impact on the catalytic behaviour of metallic nanoparticles, might they be native ligands for colloidal nanoparticles,[22] substrates of the catalytic reaction[23] or added Lewis acid or bases.[21] For example, Guo *et al.* evidenced both experimentally and computationally the hydrogenation ability of gold nanoparticles in

presence of small imines.[24] This new reactivity was attributed to a synergetic activation of H_2 by the gold surface and imines whose tight adsorption was prevented by electronic repulsion. The authors compared such reactivity to these of Frustrated Lewis Pairs (FLP) catalysts, which are able to activate small molecules in mild conditions.[25,26] However, in this case the frustration did not originate from steric repulsion between bulky Lewis acid and bases but from electronic repulsion. Later Rossi *et al.* reported a gold catalyst, decorated by amine ligands for the semi-hydrogenation of alkynes.[27] The hemilabile di-amines were able to coordinate the surface while activating H_2. Recently, our group proposed a transition metal-based semi-heterogeneous FLP catalyst formed between a NiCo surface and phosphines for the activation of phenylsilane during the hydrosilylation of benzaldehyde.[28] Indeed, the catalytic activity only appeared when combining the Lewis acid NiCo surface with a Lewis basic phosphine. Moreover, an optimal catalytic activity could be reached for a limited range of Tolman cone angles (130°-150°), suggesting that the steric hindrance around the catalytic site is of paramount importance. Yet, the challenge remains to discriminate the role of the local environment of metal sites in multimetallic compounds such as these NiCo nanoparticles.

The present work aims at providing a deeper understanding of the nature of this catalytic active site for phenylsilane activation, based on an experimental approach. For NiCo nanoparticles, we recently developed a synthetic route that allows the controlled deposition of cobalt on a *fcc* Ni core.[29] We propose here to investigate the catalytic activity of NiCo nanoparticles with a controlled sub-stoichiometric amount of Co surface sites to better understand the influence of their close environment (Co-rich or Ni-rich). We showed that the trend in phenylsilane conversion is consistent with cobalt being more active when surrounded by a Co-rich environment. This was consistently observed with two phosphine ligands, PPh_3 and P*n*Bu_3, while the first allowed a higher conversion rate than the second.

Results and discussion

Synthesis and characterization of $NiCo_x$ nanoparticles with x = 0.1, 0.2 or 1.0

NiCo nanoparticles with thin shells. NiCo nanoparticles (NPs) with low cobalt amounts were synthesized by modifying a one-pot two-step protocol (Figure 1A) developed for NiCo nanoparticles with Co/Ni = 1, for which the synthetic parameters were studied in detail.[29,30] Briefly, Ni NPs were formed during a first step by the reduction of $Ni(acac)_2$ with oleylamine (OAm, 22 equiv.) in the presence of tri-*n*-octylphosphine (TOP, 3 equiv.) at 220 °C for 2 h, under a nitrogen atmosphere.[31] The reaction mixture was cooled to room temperature. $Co_2(CO)_8$ (in chosen stoichiometry) was added to the reaction mixture, which was heated to 120 °C for 20 minutes to ensure complete dissolution of the cobalt precursor and then heated to 180 °C for 1 h. NiCo nanoparticles were isolated by centrifugation and washed with THF and EtOH (Figure 1). By tuning the quantity of the cobalt precursor introduced during the second step, a cobalt shell with chosen thickness was deposited on the Ni core. Two Co/Ni ratio (x) were used: 0.1 and 0.2, and the nanoparticles were compared with the Ni NPs obtained at the end of the first step (labelled x = 0, no shell). They were also compared with NiCo nanoparticles prepared with the same amount of TOP (3 equiv.) and OAm (22 equiv.), similar to these of our previous study[29] (x = 1.0, thick shell, TEM and XPS showed on Figure S1 and S2, respectively). All these nanoparticles present close enough average size and size distribution, meaning that they develop a similar specific surface area.

Characterization of the nanoparticles. Based on our recent work with x = 1.0, for samples with x = 0.1 and 0.2 we expected the cobalt atoms to deposit at the surface of the nickel nanoparticles. In order to verify this, we first performed chemical analysis, using two methods: energy dispersive X-ray spectroscopy (EDS) on a scanning electron microscope (SEM) and X-ray fluorescence spectroscopy (XRF) (Table 1). Both techniques provided fairly

similar results, considering that they were operated under different conditions (raw powder for SEM-EDS, pellets on cellulose for XRF) and suffer from different biases. For both samples, the Co/Ni observed in the NiCo NPs is consistent with a quasi-quantitative incorporation of the cobalt in the final sample powders.

A geometrical model allowed estimating the Co shell thickness for Co/Ni ratio from 0.1 to 1.0 (Figure 1F, see SI section 4 for the model description). A monolayer of Co (0.33 nm thick) is expected to be deposited for $x = 0.2$ while the shell thickness is expected to be 1.4 nm for $x = 1.0$. For $x = 0.1$, there is not enough cobalt to form a full monolayer, so a non-continuous shell is expected.

Transmission electron microscopy (TEM) was performed on the samples with $x = 0.1$ and 0.2 (Figure 1C and D, respectively) and compared with these of Ni NPs ($x = 0$, Figure 1B) and $x = 1.0$ sample (Figure S1). Like the Ni NPs, the NiCo nanoparticles showed a spherical morphology. The average diameters were 13.2 ± 1.5 nm and 11.9 ± 1.1 nm for $x = 0.1$ and $x = 0.2$, respectively (Figure 1E). With such size distribution, TEM does not allow to comment on the shell thickness variation from the first to the second sample. However, it can be noted that these diameters might be slightly higher than these of the Ni NPs (10.5 ± 1.2 nm), consistently with the formation of a cobalt shell, which is in agreement with our previous work on thicker shells.[29] The shell thickness is moreover consistent with these expected from our geometrical model. In agreement with the presence of a thin cobalt shell, no crystalline cobalt phase was detected by X-ray diffraction on powder (showed on Figure S3). All samples presented the most intense peak of Ni fcc (at ca 44 °) but the Scherrer length of $NiCo_0$ and $NiCo_{0.2}$ was about 1.5 nm (see Table S2). In these cases, the Ni core is quasi amorphous which is not surprising considering the high amount of TOP used in the synthesis. Although the average crystallite size of our samples could not be related to the Co/Ni ratio, the nanoparticles were in every case polycrystalline.

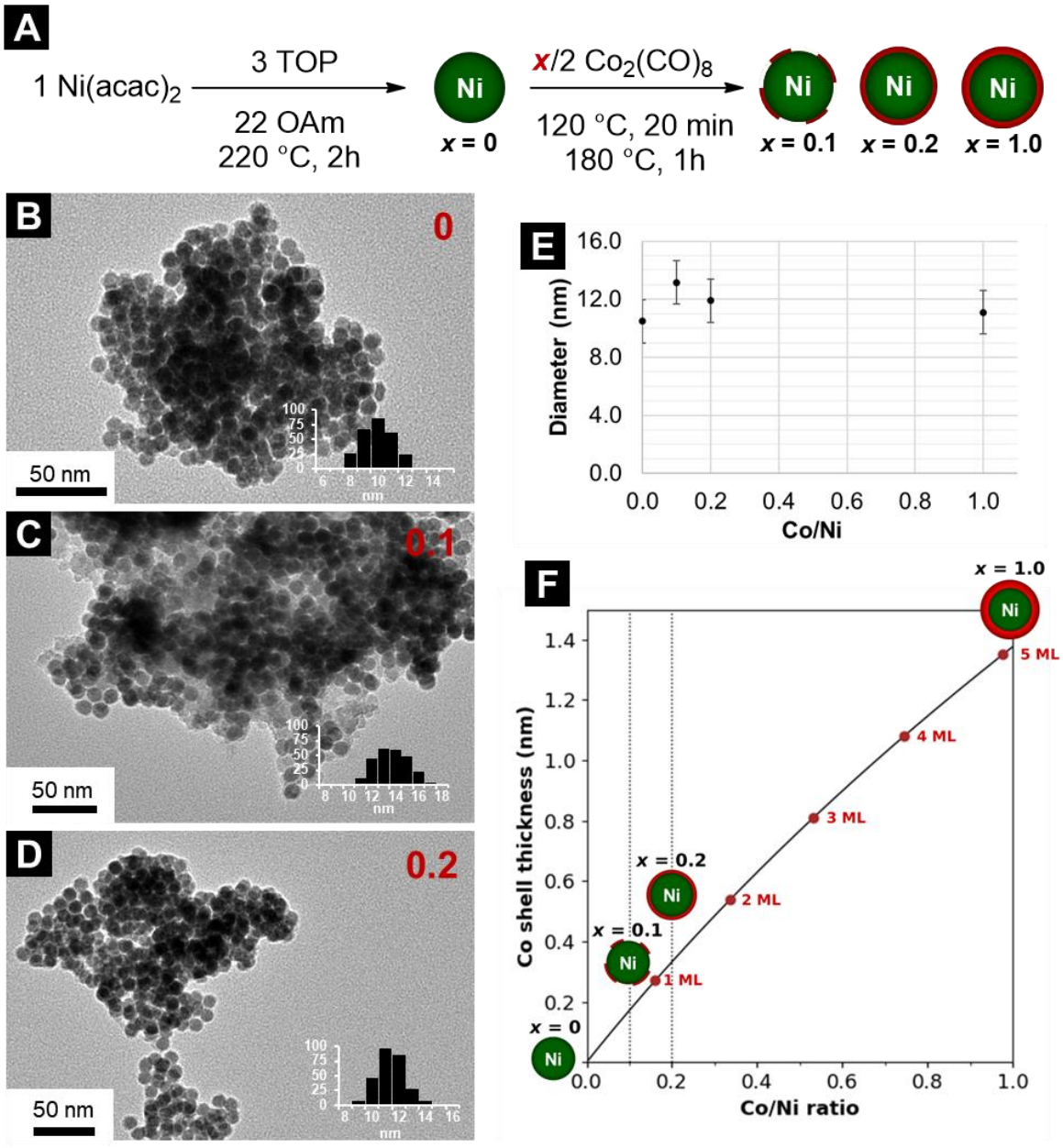

Figure 1. (A) Two-step synthesis of $NiCo_x$ nanoparticles. TEM pictures and size distributions for samples with various Co/Ni ratio (B) x = 0, (C) x = 0.1, (D) x = 0.2. (E) Average diameters and (F) geometrical model of the Co shell thickness related to the Co/Ni ratio, where each red dot from left to right shows the formation of successive monolayers (ML).

Co/Ni ratio			
Synthesis	SEM-EDS	XRF	XPS Ni-Co 3p
0.10	0.08	0.08	0.14
0.20	0.16	0.18	0.19
1.00	1.03	1.12	0.99

Table 1. Quantification of Co/Ni ratio with three methods (SEM-EDS, XRF and XPS).

Because of the low contrast between Co and Ni, the very low thickness of the shell and the large ligand amount, chemical mapping techniques such as EDS performed in scanning transmission electron mode, or high-angle annular dark field, were not enough sensitive for precise elemental composition determination. Rather, X-ray photoelectron spectroscopy (XPS) was used as a surface-sensitive and chemically-resolved spectroscopy.

XPS of the NiCo 3p, P 2p, Ni 2p, and Co 2p regions for samples with $x = 0.1$ and 0.2 is presented in Figure 2 in comparison with these of the Ni nanoparticles ($x = 0$). It confirmed the formation of an oxidized layer on the surface of the nanoparticles. The spectra were analyzed with CasaXPS following the methodology of our previous works[30,32–35] and fitting parameters can be found in the SI. The Ni 2p region (Figure 2C) was fitted with two components:[36] metallic nickel at a binding energy (B.E.) of 852.3 – 852.7 eV (dark green) and NiO (B.E. 855.6 – 855.9 eV, light green). The Co 2p region was fitted with three components:[36] metallic cobalt (B.E. 777.8 – 778.1 eV, dark red), CoO and Co_3O_4 (both around 780.9 eV, light red). The P 2p region was fitted with doublets with a splitting of 0.85 eV (Figure 2B). It presented the features of reduced P species (129.1 – 129.4 eV, dark blue) at binding energies lower than elemental P (130.0 eV), and two types of oxidized P species. The first (130.2 – 131.0 eV, blue) was attributed to TOP bound to the surface. The second (132.7 – 133.0 eV, light blue) stemmed from phosphate or tri-*n*-octylphosphine oxide (TOPO) produced by the oxidation of TOP.[35]

The oxidized species observed for Ni (light green), Co (light red) and P (light blue), were expected as they were possibly formed during the synthesis and/or as the result of the washing

in air. However the presence of these species was not an issue for the catalytic reaction: since it was conducted in reducing conditions, it is expected that the surface state presents less oxidized species, as evidenced previously by near-ambient pressure XPS on NiCo NPs[33] and in agreement with our recent work.[28] Moreover, the presence of reduced P species of phosphide type suggested that some P was incorporated in the metallic surface, a phenomenon previously observed on NiCo nanoparticles.[37]

The XPS region from 56 to 76 eV (Figure 2A) is of huge interest for these samples since it corresponds to the 3p region for both Co (56 – 64 eV) and Ni (64 – 76 eV). This region was fitted as in our previous studies[37] and confirmed the presence of both reduced metals (Ni in dark green, Co in dark red) as well as oxidized ones (Ni in light green, Co in light red) although the deconvolution was less precise than for the 2p regions due to the overlap of the peaks. Most importantly, this region allows directly comparing the relative amount of Ni and Co on the surface, with an inelastic mean free path (IMFP) of ca 19 – 20 nm. The last column of Table 1 indicates the observed ratio based on the Co and Ni peak areas. The surface ratios were slightly higher than the average Co/Ni ratio in both samples, which is consistent with the fact that Co was on top of the Ni core.

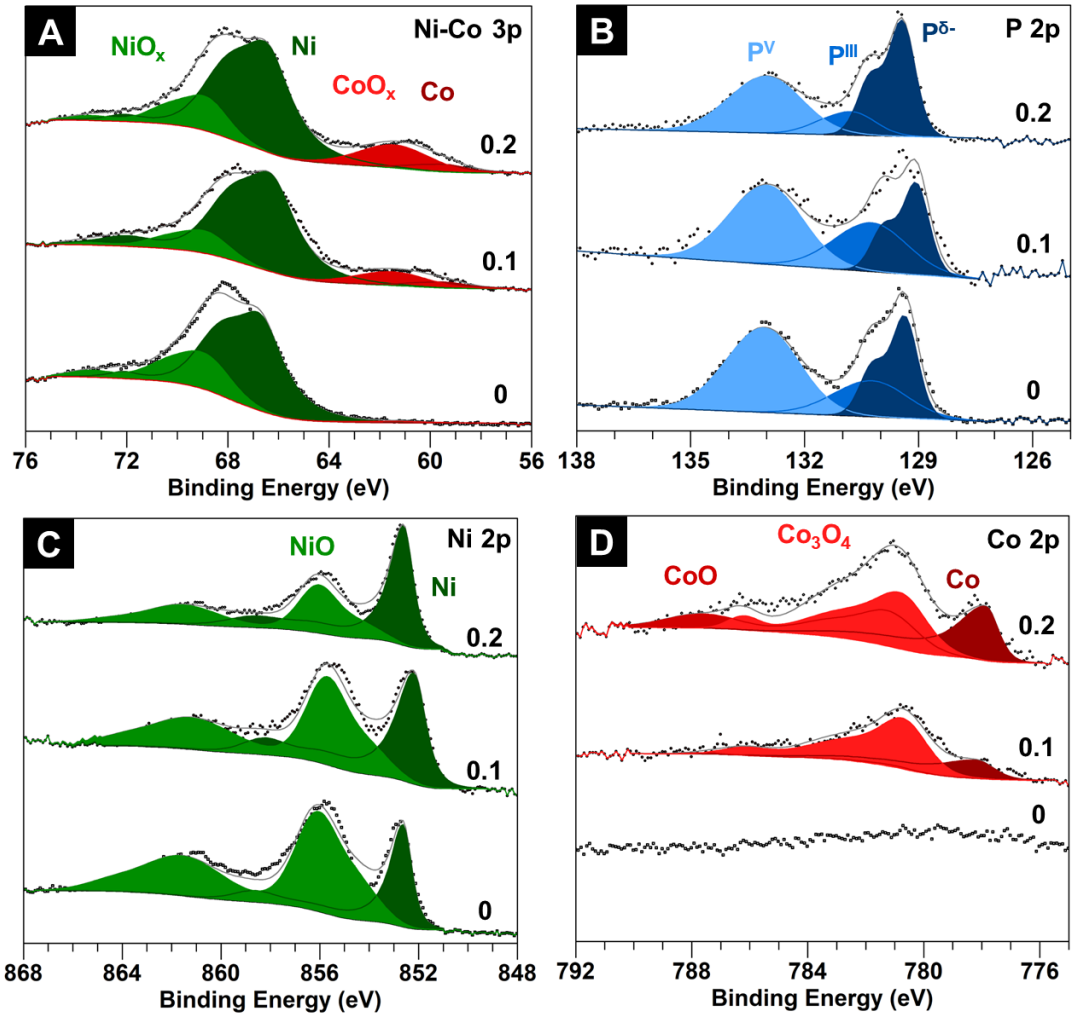

Figure 2. X-ray Photoelectron Spectra of samples with x = 0, 0.1 and 0.2, for (A) Ni-Co 3p region, (B) P 2p region, (C) Ni 2p region and (D) Co 2p region.

Altogether, XPS confirmed that the samples with x = 0.1 and 0.2 presented a surface with species that are similar with these of the x = 1.0 sample studied before, with the amount of cobalt as the variable parameter. In all cases, the surface is cobalt-rich with coexistence of reduced and oxidized species. XPS also confirmed the expected trend in terms of Co abundance, which is significantly lower for x = 0.1 than for x = 0.2, consistently with the geometric model. Thus, these samples were investigated for the activation of Si–H bond of phenylsilane in the presence of an additional phosphine and we looked for the influence of the Co/Ni ratio on the catalytic activity.

Influence of the Co/Ni ratio on the catalytic conversion of phenylsilane

Catalytic reaction. Our previous study for Co/Ni = 1.0 showed an optimal catalytic activity in the presence of an additional phosphine, for a limited range of Tolman cone angles: 130 – 150 °.[28] Therefore, we selected triphenylphosphine (145 °) and tri-*n*-butylphosphine (132 °) for evaluating the influence of the Co/Ni ratio. The catalytic reaction was the Si–H activation of phenylsilane, resulting in the hydrosilylation (partial or total) of benzaldehyde (Scheme 1, see experimental section for details). It was performed with the two main samples with $x = 0.1$ and 0.2, and for comparison with the two references samples with $x = 0$ and 1.0. All experiments were carried with a constant total metal charge of 20 mol% (2 mg), consistently with our preliminary work.[28] The phenylsilane conversions, measured by ^{1}H NMR using mesitylene as internal standard, are indicated in Table 2 for experiments without phosphine or with one of the two phosphines of interest (a typical NMR spectrum is showed on Figure S4).

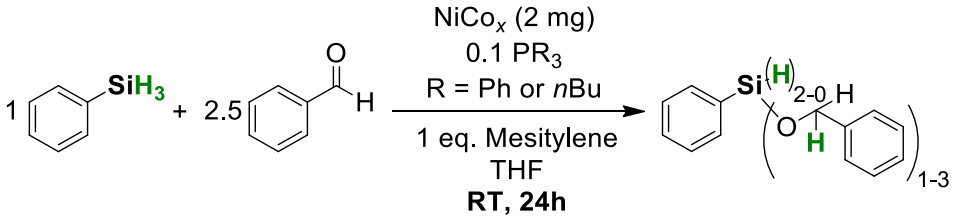

Scheme 1. Catalytic conversion of phenylsilane in the presence of $NiCo_x$ NPs and a phosphine.

Entry	**Co/Ni**	**$PhSiH_3$ conv. (%)**		
		-	PPh_3	$PnBu_3$
1	1.0	0	100	57
2	0.2	ε	16	11
3	0.1	ε	2	2
4	0	ε	ε	ε

Table 2. Phenylsilane conversion measured by ^{1}H NMR with mesitylene as an internal standard (ε stands for traces conversion).

As expected, the reactions conducted in the absence of phosphine yielded no significant conversion (Table 2, first column, entries ***1*** to ***4***). In addition, the absence of cobalt in the sample led to no conversion (entry ***4***), regardless of the presence of phosphine, which was consistent with our previous work.

In the presence of PPh_3, the phosphine expected to be the most efficient due to its optimal Tolman cone angle, the sample with $x = 1.0$ showed a quantitative conversion (expected from our previous study). A low conversion of 2 % was found for the $x = 0.1$ sample (entry ***3***) and a significantly higher one of 16 % was found for the $x = 0.2$ sample (entry ***2***). Thus, the conversion increased with the amount of Co.

A similar trend was observed for the reaction conducted with P*n*Bu_3, although the conversions were generally lower: 2 %, 11 % and 57 % for $x = 0.1$, 0.2 and 1.0, respectively. This confirmed that the cobalt amount and/or the Co/Ni ratio have a significant influence on the catalytic reaction.

Because the presence of cobalt atoms was a requirement for the Si–H activation to proceed, we decided to re-examine these data while considering that surface Co was the active site.

As the Co amount in the catalyst varied between the experiments, we normalized the phenylsilane consumption by the total Co amount for each catalyst, as described in the SI (see Section 5). Decreasing the Co/Ni ratio of core-shell NiCo nanoparticles resulted in Co-poor surfaces, as schematized on Figure 3C, until reaching a cobalt-free surface (case ***(a)***). In the case of a submonolayer of cobalt ($x = 0.1$), the cobalt atoms may not be neighbors to each other ***(b)***, or alternatively, they may form small islands ***(c)***. When the amount of cobalt is above one monolayer ($x = 0.2$ and 1.0), a continuous Co shell can be formed ***(d)***, or alternatively, a less regular shell with some richer and some poorer-containing cobalt regions may co-exist ***(e)***. The quality of our TEM data does not allow to make a final assessment, but

we can propose as a reasonable hypothesis that the higher the x value, the richer in Co the environment for a given cobalt active site. Furthermore, once the first cobalt monolayer is formed ($x = 0.2$), the number of cobalt surface active sites remains constant.

If the active sites were not influenced by their close environment, we expected to differentiate two regimes as depicted in Figure 3D (grey dashed line). At low x ($x < 0.2$), the catalyst would present only accessible surface Co because Co is expected to be deposited homogeneously on the Ni core and because there is not enough Co to form a monolayer. All Co should be accessible and sharing the same intrinsic activity. Thus, the normalized catalytic activity (by mol of Co) should be a plateau in this first regime. At higher x ($x > 0.2$), samples contained enough Co to form at least one complete Co layer. An increasing amount of Co becomes non-accessible, buried under the external active Co layer. The normalized catalytic activity should therefore slightly decrease in this second regime. Such trends were not observed. Rather, regardless of the phosphine, the normalized activity increased with increasing Co amount (Figure 3B).

We suggested that the close environment of the Co surface active sites could influence their intrinsic activity. *If a Ni-environment positively stimulated the Co active sites*, we would expect a catalytic activity maximum for a sample exhibiting less than a Co monolayer (Figure 3D, green dashed line). This was also not observed, ruling out this hypothesis. On the contrary, for the two phosphines tested, the normalized activity increased over the whole range tested, suggesting that the enrichment of the Co active sites' environment in cobalt stimulated their catalytic activity (Figure 3D, red line). The catalytic activity increased however slower for samples exhibiting increasing amounts of inaccessible Co. Altogether, the results suggest that the catalytic activity of $NiCo_x$ nanoparticles for Si–H activation is

enhanced when the surface cobalt sites are in a Co-rich environment, close to the one of a pure Co surface.

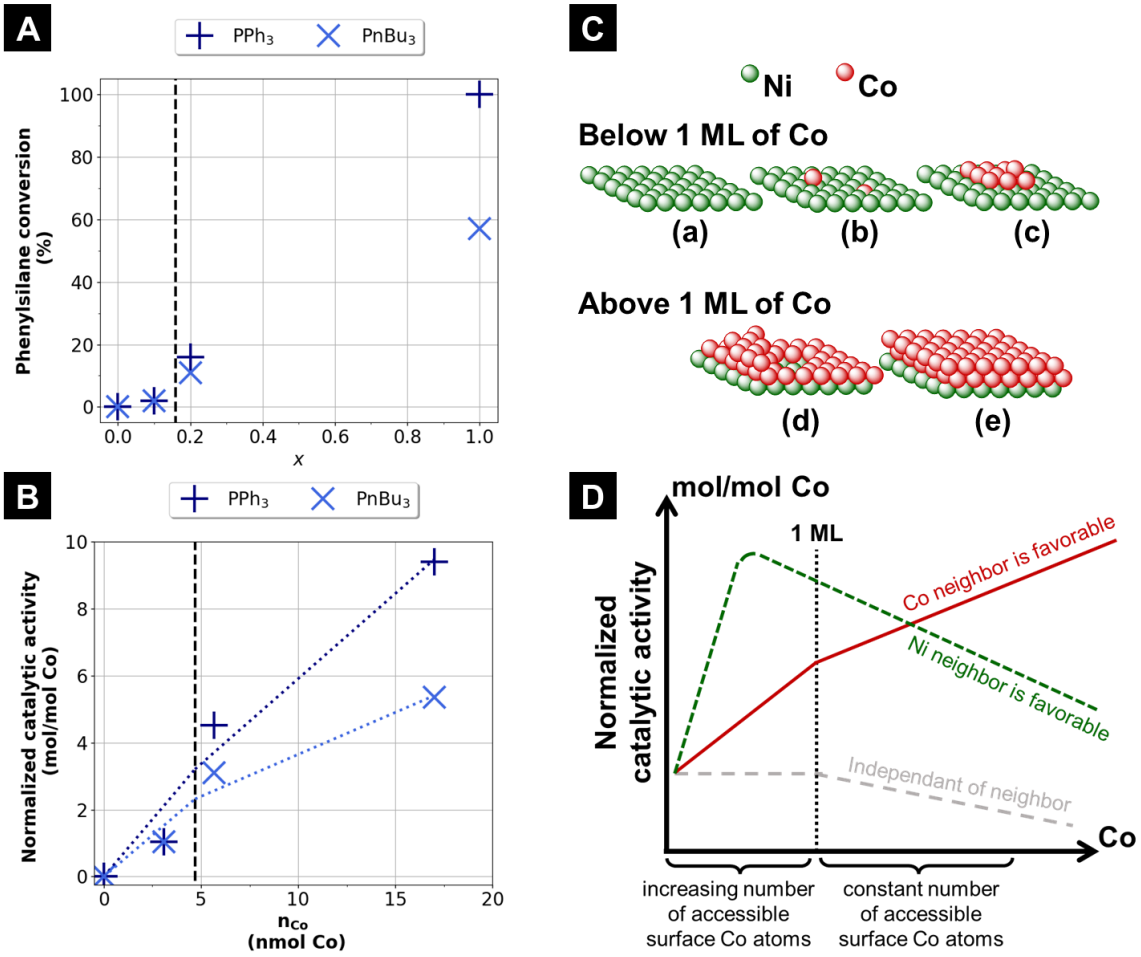

Figure 3. (A) Graphical representation of phenylsilane conversion, (B) Normalized catalytic activity (mol $PhSiH_3$ consummed/mol Co, dotted vertical line indicates the theoretical position of the monolayer), (C) schematic representation of a nickel surface covered with an increasing number of Co atoms up to a Co multilayer and (D) expected evolution of the normalized catalytic activity depending on the total Co amount and its accessibility.

Conclusion

In conclusion, we gained a better understanding of the nature of the active site of bimetallic NiCo nanoparticles for phosphine-assisted hydrosilylation. By varying the ratio cobalt/nickel

introduced in a two-step colloidal synthesis, we tuned the cobalt content of the nanoparticle's surface. We compared the catalytic activity of cobalt-free nickel surfaces, nickel surfaces decorated by cobalt islands and pure cobalt surface covering a nickel core. For both phosphines used as molecular partner to the metallic catalyst, the catalytic activity for the hydrosilylation of benzaldehyde by phenylsilane decreases sharply when the surface cobalt content was reduced. This ruled out a synergistic effect between nickel and cobalt because it would have resulted in an activity optimum for intermediate surface amounts of cobalt. Rather, we showed that the most beneficial configuration was a cobalt site sitting in a cobalt-rich environment.

In the future, developing a synthesis of morphologically similar cobalt nanoparticles would allow comparing the influence of the Ni and Co cores on the surface activity of cobalt. Moreover, now that the catalytic activity has been clarified from the point of view of the surface, it would be of great interest to understand the catalytic activation mechanism involving a phosphine with controlled steric hindrance. DFT computations on such a system could lead to new insights for understanding the role of phosphines as molecular partner to enhance the activity of metallic nanoparticle catalysts.

Experimental section

Reagents and general information. Oleylamine (OAm; 98%), benzaldehyde (99.5%), phenylsilane ($PhSiH_3$; 97%), triphenylphosphine (PPh_3; 99%) anhydrous tetrahydrofuran (THF; 99.99%, inhibitor free) and mesitylene (Mes; 98%, dried and degassed prior to utilization) were purchased from Sigma-Aldrich. Tri-n-octylphosphine (TOP; 97%), tri-*n*-butylphosphine ($PnBu_3$; 99%), dicobalt(0) octacarbonyl ($Co_2(CO)_8$; >95%), and nickel(II) acetylacetonate ($Ni(acac)_2$; anhydrous, min. 95%) were purchased from Strem Chemicals and stored in a glovebox. Deuterated chloroform ($CDCl_3$; 99.5%) was purchased from Euriso-top.

All chemicals described above were used without further purification. Glassware was kept in an oven at 120 °C prior to utilization.

General procedure for the synthesis of NiCo nanoparticles. $NiCo_x$ were synthesized according a one-pot two-step colloidal synthesis, depositing a cobalt shell on preformed Ni nanoparticles. The glassware was taken out from the oven and a three-neck round bottom flask equipped with a temperature finger and an air cooler was charged with the oleylamine (22 equiv., 27 mL) which was subjected to three cycles vacuum/N_2 to degas as much as possible. $Ni(acac)_2$ (1 equiv., 3.73 mmol, 958 mg) and tri-*n*-octylphosphine (3 equiv., 5 mL) were collected in the glovebox and added under N_2 to the flask containing oleylamine. The mixture was once again subjected to three cycles of vacuum/N_2 and thereafter heated up to 220°C. After 2 hours, the mixture was cooled to room temperature. $Co_2(CO)_8$ (x/2 equiv., x = 0, 0.1, 0.2, 1.0) was added to the mixture which was heated to 120 °C for 20 minutes, then to 180 °C for 1h (short heating program). Thereafter the mixture was cooled back to room temperature and washed three times distributing the reaction mixture in four 50 mL centrifugation tubes. Nanoparticles were redispersed with 10 mL THF and 30 mL EtOH was then added to foster aggregation before centrifugating at 9000 rpm for 10 min.

Hydrosilylation of benzaldehyde by phenylsilane. In the glovebox, 10 mL vials were charged with phenylsilane (1 equiv., 0.16 mmol, 40 µL), benzaldehyde (2.5 equiv., 20 µL), mesitylene as internal standard (1 equiv., 22 µL) and 2 mL THF. A catalytic amount of nanoparticles (2 mg) and triphenylphosphine (0.1 equiv., 4 mg) or tri-*n*-butylphosphine (0.1 equiv., 3 mg) were then added. After 22 hours, ^1H NMR tubes were prepared by diluting a drop of the reaction mixture in $CDCl_3$.

Acknowledgements

This project has received funding from the European Research Council (ERC) under the European Union's Horizon 2020 research and innovation programme (grant agreement No 758480). Antoine Miche (Sorbonne Université, CNRS, Fédération de Chimie et Matériaux de Paris-Centre, LRS) is acknowledged for the XPS measurements.

References

[1] Y. L. Fang, J. T. Miller, N. Guo, K. N. Heck, P. J. J. Alvarez, M. S. Wong, *Catal. Today* **2011**, *160*, 96–102.

[2] A. K. Singh, Q. Xu, *ChemCatChem* **2013**, *5*, 652–676.

[3] P. Liu, J. K. Nørskov, *Phys. Chem. Chem. Phys.* **2001**, *3*, 3814–3818.

[4] L. Carbone, P. D. Cozzoli, *Nano Today* **2010**, *5*, 449–493.

[5] A. Zaleska-Medynska, M. Marchelek, M. Diak, E. Grabowska, *Adv. Colloid Interface Sci.* **2016**, *229*, 80–107.

[6] F. Maroun, F. Ozanam, O. M. Magnussen, R. J. Behm, *Science (80-.).* **2001**, *293*, 1811–1814.

[7] K. G. Papanikolaou, M. T. Darby, M. Stamatakis, *ACS Catal.* **2020**, *10*, 1224–1236.

[8] N. Marcella, J. S. Lim, A. M. Płonka, G. Yan, C. J. Owen, J. E. S. van der Hoeven, A. C. Foucher, H. T. Ngan, S. B. Torrisi, N. S. Marinkovic, E. A. Stach, J. F. Weaver, J. Aizenberg, P. Sautet, B. Kozinsky, A. I. Frenkel, *Nat. Commun.* **2022**, *13*, 1–9.

[9] B. AlSabban, L. Falivene, S. M. Kozlov, A. Aguilar-Tapia, S. Ould-Chikh, J. L. Hazemann, L. Cavallo, J. M. Basset, K. Takanabe, *Appl. Catal. B Environ.* **2017**, *213*, 177–189.

[10] L. Li, D. H. Anjum, H. Zhu, Y. Saih, P. V. Laveille, L. D'Souza, J. M. Basset, *ChemCatChem* **2015**, *7*, 427–433.

[11] D. San-José-Alonso, J. Juan-Juan, M. J. Illán-Gómez, M. C. Román-Martínez, *Appl. Catal. A Gen.* **2009**, *371*, 54–59.

[12] J. Horlyck, C. Lawrey, E. C. Lovell, R. Amal, J. Scott, *Chem. Eng. J.* **2018**, *352*, 572–580.

[13] T. Saelee, M. Lerdpongsiripaisarn, M. Rittiruam, S. Somdee, A. Liu, S. Praserthdam, P. Praserthdam, *Sci. Rep.* **2021**, *11*, 1–17.

[14] J. López-Tinoco, R. Mendoza-Cruz, L. Bazán-Díaz, S. C. Karuturi, M. Martinelli, D. C. Cronauer, A. J. Kropf, C. L. Marshall, G. Jacobs, *Catalysts* **2019**, *10*, 18.

[15] J. Parikh, S. Srivastava, G. C. Jadeja, *Ind. Eng. Chem. Res.* **2019**, *58*, 16138–16152.

[16] L. J. Malobela, J. Heveling, W. G. Augustyn, L. M. Cele, *Ind. Eng. Chem. Res.* **2014**, *53*, 13910–13919.

[17] L. Wang, S. He, L. Wang, Y. Lei, X. Meng, F. S. Xiao, *ACS Catal.* **2019**, *9*, 11335–11340.

[18] H. Miao, K. Ma, H. Zhu, K. Yin, Y. Zhang, Y. Cui, *RSC Adv.* **2019**, *9*, 14580–14585.

[19] B. Chen, F. Li, G. Yuan, *Catal. Letters* **2017**, *147*, 2877–2885.

[20] G. A. Gebreslase, M. V. Martínez-Huerta, M. J. Lázaro, *J. Energy Chem.* **2022**, *67*, 101–137.

[21] A. Palazzolo, S. Carenco, *Chem. Mater.* **2021**, acs.chemmater.1c03105.

[22] J. R. Pankhurst, P. Iyengar, A. Loiudice, M. Mensi, R. Buonsanti, *Chem. Sci.* **2020**, *11*, 9296–9302.

[23] C. Schröder, A. K. Baumann, M. C. Schmidt, J. Smyczek, P. A. Haugg, O. C. Graap, S. Schauermann, *J. Phys. Chem. C* **2022**, DOI 10.1021/acs.jpcc.2c00987.

[24] G. Lu, P. Zhang, D. Sun, L. Wang, K. Zhou, Z. X. Wang, G. C. Guo, *Chem. Sci.* **2014**, *5*, 1082–1090.

[25] D. W. Stephan, G. Erker, *Chem. Sci.* **2014**, *5*, 2625–2641.

[26] R. Pal, M. Ghara, P. K. Chattaraj, *Catalysts* **2022**, *12*, 201.

[27] J. L. Fiorio, N. López, L. M. Rossi, *ACS Catal.* **2017**, *7*, 2973–2980.

[28] A. Palazzolo, S. Carenco, *Chem. Mater.* **2021**, *33*, 7914–7922.

[29] A. Palazzolo, C. Poucin, A. P. Freitas, A. Ropp, C. Bouillet, O. Ersen, S. Carenco, *Nanoscale* **2022**, DOI 10.1039/D2NR00917J.

[30] S. Carenco, C. H. Wu, A. Shavorskiy, S. Alayoglu, G. A. Somorjai, H. Bluhm, M. Salmeron, *Small* **2015**, *11*, 3045–3053.

[31] S. Carenco, C. Boissière, L. Nicole, C. Sanchez, P. Le Floch, N. Mézailles, *Chem. Mater.* **2010**, *22*, 1340–1349.

[32] C. S. Bonifacio, S. Carenco, C. H. Wu, S. D. House, H. Bluhm, J. C. Yang, *Chem. Mater.* **2015**, *27*, 6960–6968.

[33] S. Carenco, C. S. Bonifacio, J. C. Yang, *Chem. - A Eur. J.* **2018**, *24*, 12037–12043.

[34] J. Kolny-Olesiak, *Zeitschrift fur Naturforsch. - Sect. A J. Phys. Sci.* **2019**, *74*, 709–719.

[35] S. Carenco, Z. Liu, M. Salmeron, *ChemCatChem* **2017**, *9*, 2318–2323.

[36] M. C. Biesinger, B. P. Payne, A. P. Grosvenor, L. W. M. Lau, A. R. Gerson, R. S. C. Smart, *Appl. Surf. Sci.* **2011**, *257*, 2717–2730.

[37] L. M. Moreau, D.-H. H. Ha, C. R. Bealing, H. Zhang, R. G. Hennig, R. D. Robinson, *Nano Lett.* **2012**, *12*, 4530–4539.

Twitter

@SophieCARENCO @lcmcp_paris

TOC graphic

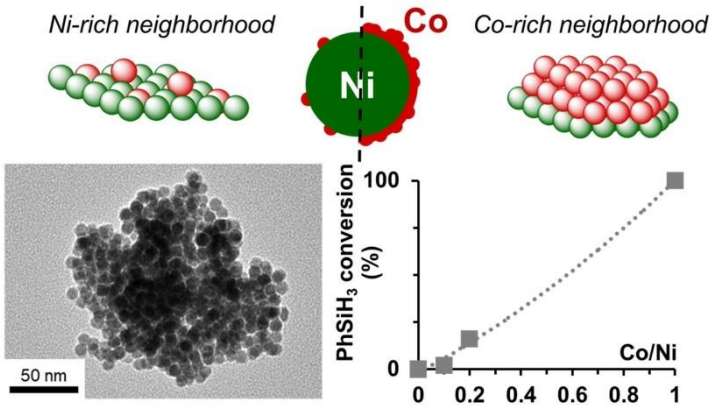

The intrinsic activity of a cobalt surface site, sitting on a nickel nanoparticle, is comparatively higher when its neighbours are cobalt atoms *vs.* nickel atoms.